Very-Low-Driving-Voltage Electroabsorption Modulators Operating at 40 Gb/s

Hideki Fukano, Takayuki Yamanaka, Munehisa Tamura, and Yasuhiro Kondo

***Abstract*—This paper has demonstrated a 40-Gb/s low-driving-voltage electroabsorption modulator (EAM) having InGaAlAs/InAlAs multiquantum-well active core. A narrow core buried with polyimide provides a strong optical and electrical confinement, resulting in a maintained large extinction ratio (ER) and an increased 3-dB down frequency. The fabricated EAM shows a 3-dB down frequency as large as 46 GHz, even for the active-core length as long as 200 μm. The EAM operates at 40 Gb/s with an RF ER of 10.5 dB at a driving voltage as low as 0.79 V.**

***Index Terms*—Electroabsorption, electroabsorption modulator (EAM), InGaAlAs/InGaAs, low-driving voltage.**

I. Introduction

THE EXPLOSIVE increase of a data traffic on the Internet has led to a demand for low-cost large-capacity optical transmission systems, even in metro or intraoffice applications. An electroabsorption modulator (EAM) is a promising transmitter-device for 40-Gb/s very-short-reach optical link applications because of its compactness and ease of operation [1]–[9]. In such applications, power consumption is a key issue for the wide use of 40-Gb/s EAMs. Reducing driving voltage is a very effective way to not only reduce the power consumption of EAM itself but also to reduce that of the Peltier cooler, which uses a lot of power in keeping the temperature of EAM constant. However, reported EAM driving voltages (Vpps) under the normal 50-Ω termination condition remain over 2 V. A low-voltage driver generally consumes low power, resulting in a large reduction in the total power consumption of the transmitter module. Recent progress in Si–Ge technology has made 40-Gb/s logic ICs possible [10]. A low Vpp would enable the integration of logic ICs and driving circuits on one chip using Si–Ge technologies, which would greatly reduce power consumption, cost, and size, as well as improve the microwave-transmission characteristics because the components (bonding wire, waveguide, dc-block, etc) between the driving circuits and logic ICs could be eliminated.

Since the InGaAlAs multiquantum-well (MQW) system has a larger conduction bandgap offset $(\Delta E_{\rm c})$ than the InGaAsP system, the better carrier confinement in the wells produces sharp exciton absorption spectra over a wide bias range. This results in a large extinction ratio (ER) and its steep change with voltage, which are very important for lowering the driving voltage. Therefore, a significant decrease of Vpp can be achieved by properly designing an InGaAlAs-based MQW EAM so that it has steep extinction characteristics without sacrificing electrical-to-optical (E/O) 3-dB bandwidth $(f_{3\,\rm dB})$.

In this paper, we describe a successfully fabricated very low-driving-voltage EAM. Section II describes a device design for lowering the driving voltage. Section III describes the fabrication process. The characteristics of the fabricated EAM chips are shown in Section IV. The fabricated EAM exhibits 40-Gb/s operation with an RF ER of 10.5 dB at a Vpp as low as 0.79 V.

Manuscript received November 7, 2005; revised January 23, 2006.

The authors are with the NTT Photonics Laboratories, Atsugi, Kanagawa 243-0198, Japan (e-mail: fukano@aecl.ntt.co.jp; tyama@aecl.ntt.co.jp; mtamura@aecl.ntt.co.jp; kujira@aecl.ntt.co.jp).

Digital Object Identifier 10.1109/JLT.2006.872310

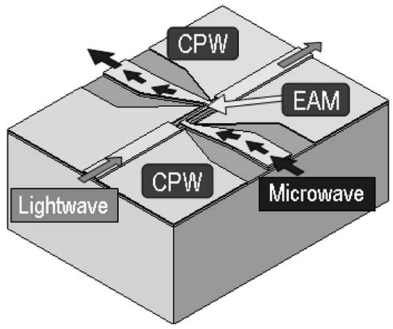

Fig. 1. Schematic view of an EAM integrated with CPWs on SI-InP substrate.

II. Device Structure and Device Design

We designed an EAM having an electrode running on the modulator active part as a microwave-transmission line with both input and output coplanar-waveguide (CPW) ports [11], as shown in Fig. 1. A CPW-electrode structure provides a feed line with a very low microwave-propagation loss. This configuration is superior to the lumped-element configuration in that it minimizes the microwave return loss because there is no significant microwave reflection point. The EAM waveguide has an active part $(L_{\rm EA})$ and passive parts at both ends. Passive parts are added for handling the chip rather than improving the device characteristics. An InGaAlAs/InAlAs MQW stack was incorporated in the modulator p-i-n optical core.

Our approach to reducing the driving voltage has two aspects. One is the material used for the EAM core, and the second is the EAM's structural design. Since InGaAsP MQWs have a small $\Delta E_{\rm c}$, the electron state is extended under a high voltage. This results in a weak quantum confined Stark effect (QCSE). However, since InGaAlAs MQWs have a large $\Delta E_{\rm c}$, the wells provide a stronger carrier confinement. This produces a confined electron state even under a high voltage, resulting in a strong QCSE over a wide range of biases. We employed tensile-strained InGaAlAs/InAlAs MQW layers [12], which show excellent extinction characteristics.

0733-8724/$20.00 © 2006 IEEE

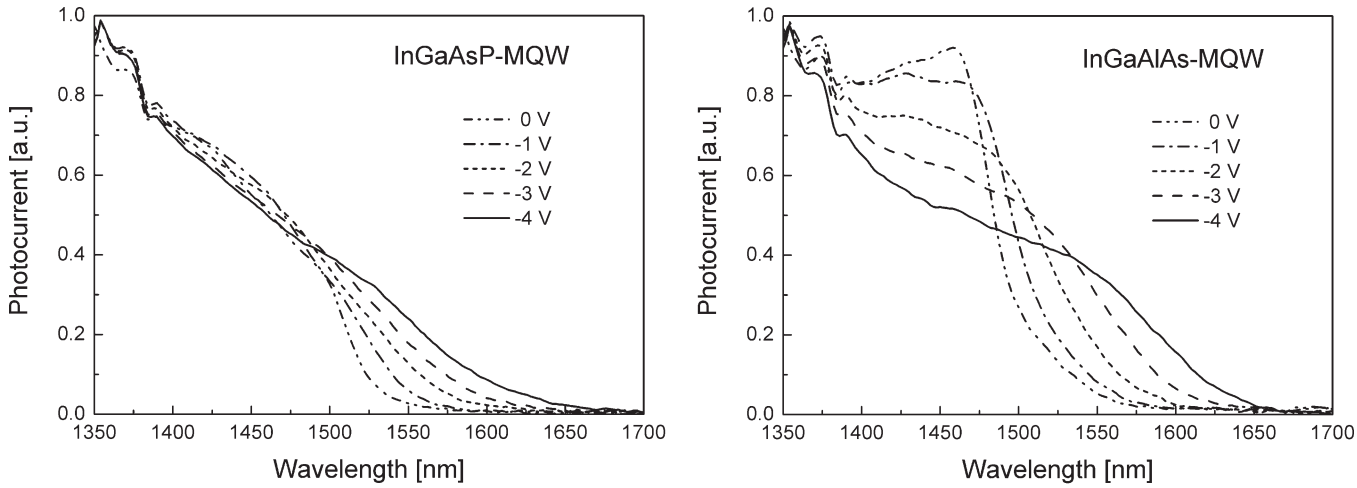

Fig. 2. Measured absorption current spectra for various voltages. (a) InGaAsP MQWs and (b) InGaAlAs MQWs.

Fig. 2 compares the measured absorption current spectra for compressive-strained InGaAsP MQWs [13] and tensile-strained InGaAlAs MQWs [12] for various voltages. Note that compressive strain generally increases ΔE_c, but tensile strain decreases it. The key feature is a spectral curve difference between them. For InGaAsP MQWs, the exciton absorption peak is not strong even at the compressive strain condition, and the change with voltage is therefore relatively small. In contrast, InGaAlAs MQWs exhibit sharper exciton absorption peaks due to the inherently large ΔE_c, resulting in a large change in absorption with voltage. This makes the ER large and the voltage dependence steep.

A proper structural design provides a larger bandwidth while lowering the microwave loss at the same time. To reduce the driving voltage, we need to boost the ER and make the slope steep while maintaining the E/O bandwidth required for 40-Gb/s operation. A simple way to do this is to increase the EA active length. However, there is a tradeoff between the ER and E/O bandwidth against modulator length. The best way to relax this tradeoff is to make the core narrower, which enlarges the E/O bandwidth, while maintaining the strong optical confinement.

To obtain the strong optical confinement, it is essential that the mesa be buried in a low-refractive-index material. For this purpose, we use polyimide. The calculation results in Fig. 3 show how the optical confinement factor (Γ) varies with core width (W_c). As W_c decreases, Γ remains almost constant, and it is still large enough at a W_c of 1 μm due to the large difference in refractive index between the core and polyimide. This suggests that as W_c decreases, the large ER is maintained, while the E/O bandwidth increases due to the smaller junction capacitance. Therefore, to reduce the driving voltage, we have to choose an optimized condition so that the ER is maximized and the $f_{3\,\mathrm{dB}}$ is kept at a sufficient value for 40 Gb/s operation, while taking into account the above tradeoff relationship.

In optimizing the tradeoff relationship, it is essential to predict the electrical-to-electrical (E/E) and E/O bandwidth precisely. To do this optimization, we used the simulation model described in [14]. The simulation result in Fig. 4 shows what

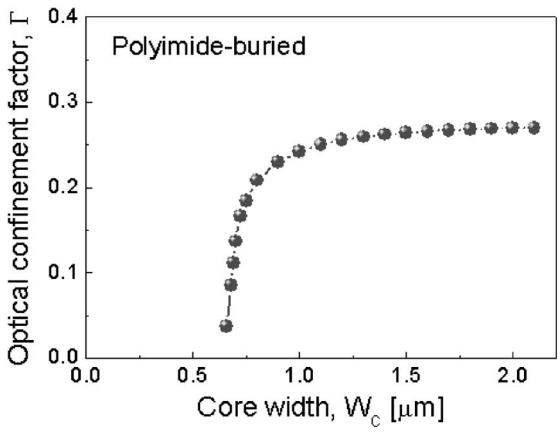

Fig. 3. Calculated optical confinement factor (Γ) versus core width (W_c).

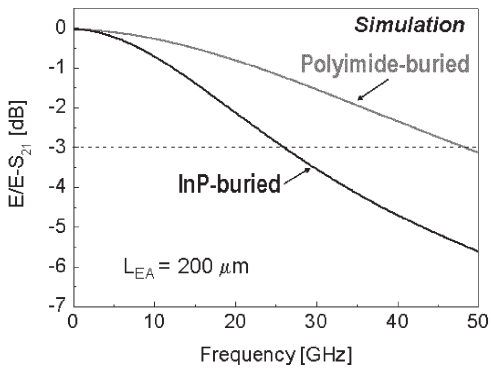

Fig. 4. Simulated microwave E/E transmission (S_{21}) for a 200-μm EAM for different burying material.

effect the burying material has on microwave E/E transmission (S_{21}) for a 200-μm-long EAM with a narrow mesa about 1-μm wide. If we use InP for the burying material, the 3-dB down bandwidth is only about 25 GHz. However, the use of polyimide significantly increases S_{21} due to its low-dielectric constant. This indicates that polyimide would also be very effective in confining microwaves in an EAM waveguide. Using

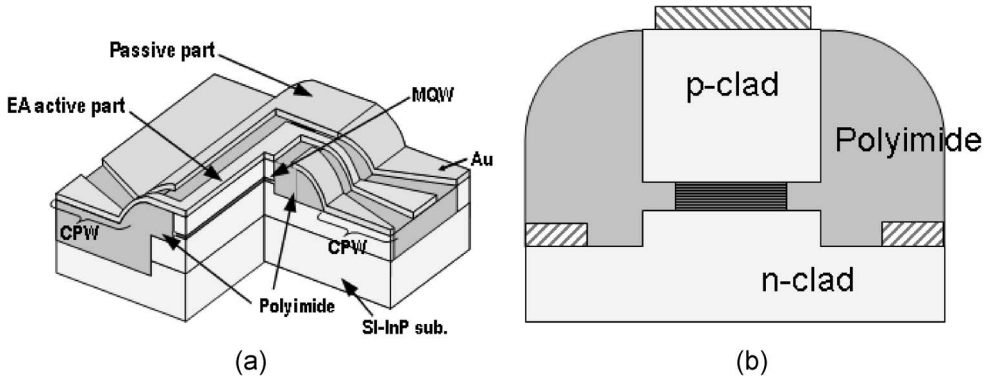

Fig. 5. (a) Schematic view and (b) cross-sectional view of the fabricated EAM.

the model, we confirmed that the 12-well-MQW EAM even with an L_{EA} as long as 200 μm could provide an $f_{3\,\mathrm{dB}}$ of more than 40 GHz by narrowing the core width.

III. Device Fabrication

Fig. 5 shows a schematic view and cross-sectional view of the fabricated EAM. The passive and active parts of the fabricated EAM have the same core structure. The passive parts are formed by electrically shortening the p- and n-layers to maintain zero bias with a low-optical loss. In this paper, we used active parts that were 50-, 75-, 100-, and 200-μm long. The double heterostructure, which consists of an n-InP cladding layer, an active layer containing InGaAlAs/InAlAs MQW layers, and a p-InP cladding layer, was grown on a semiinsulating (SI) InP substrate by using metal–organic vapor phase epitaxy (MOVPE). The MQW consists of 12 InGaAlAs wells (10.2-nm thick, 0.40% tensile strain) with InAlAs barriers (5.3-nm thick, 0.25% compressive strain). The peak photoluminescence wavelength of the MQW was 1.47 μm at room temperature. After defining the mesa by inductively coupled plasma-reactive ion etching with HBr-based gases, the core was narrowed using a side-etching technique with wet chemical solution. Side etching depth is about 0.4 μm. This is very advantageous in maintaining the low-device resistance afforded by the relatively wide mesa, while reducing the core width, as has been demonstrated in waveguide-type photodiodes using an active region undercut mesa [15], [16]. The core widths are 1.1, 1.6, and 2.1 μm. The mesa was buried using thick photo-sensitive polyimide. This provides the strong optical confinement and a low-parasitic capacitance. It also ensures a smooth electrode-metal connection between the top of the mesa and bottom of the SI substrate through the rounded edge of the polyimide. Therefore, optimized low-loss CPWs for the input and output ports connected via a microwave-transmission line on the EAM could be successfully fabricated using the metal-liftoff technique. After cleaving the wafer, both edges were antireflection coated.

IV. Fabricated Device Characteristics

Fig. 6 shows the measured relative fiber-to-fiber ER characteristics for various L_{EA}s in the case of 1.55-μm-wavelength TE-polarized light. The EAMs have an active-core width of

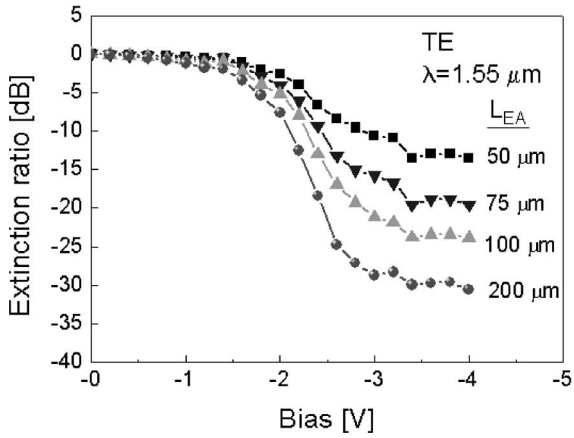

Fig. 6. Relative fiber-to-fiber ER characteristics for various active-layer lengths (L_{EA}) in the case of 1.55-μm-wavelength TE-polarized light.

1.1 μm. The longer the modulator length is, the larger the ER with very steep change. The ER of more than 18 dB was obtained even for only 1-V voltage swing (from -1.5 to -2.5 V) for an L_{EA} of 200 μm. Insertion loss without bias is about 10.6 dB, which includes coupling losses with optical fibers. The estimated insertion loss at 200-μm EAM part without bias is about 3.1 dB. These excellent characteristics clearly imply that the well-designed strained InGaAlAs/InAlAs MQW has far superior extinction, which is further enhanced by the large well number of 12.

Fig. 7 shows microwave transmission (S_{21}) and return loss (S_{11}) curves for active-layer lengths of 50, 100, and 200 μm. The EAMs again have an active-core width of 1.1 μm. As the modulator gets longer, S_{21} drops, and S_{11} increases. However, even at 200 μm, the transmission and return losses are quite low. At 50 GHz, S_{21} is still larger than -3 dB, and S_{11} remains below -10 dB. This is because of the small p-i-n capacitance due to the narrow core and the large number of wells.

Fig. 8 shows the measured relative fiber-to-fiber ER characteristics for various MQW active-core widths. There is almost no degradation of ER characteristics even at W_c as narrow as 1.1 μm. This is due to the large optical confinement in the MQW active core achieved by burying the waveguide with low-refractive-index polyimide. Reducing EAM waveguide width leads to a wider $f_{3\,\mathrm{dB}}$ because it reduces p-i-n junction capacitance as well as microwave-transmission loss at the p-clad

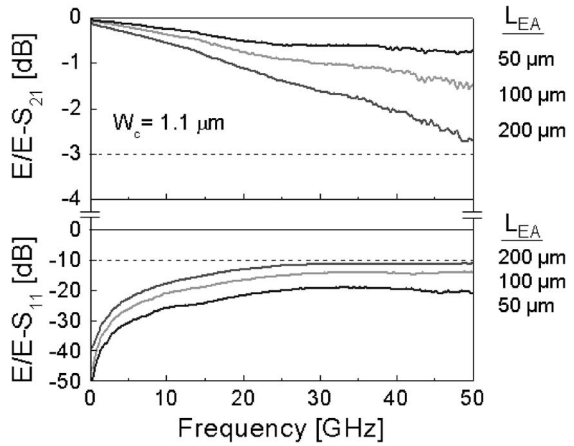

Fig. 7. Measured microwave transmission (S_{21}) and return loss (S_{11}) curves for active-layer lengths of 50, 100, and 200 μm.

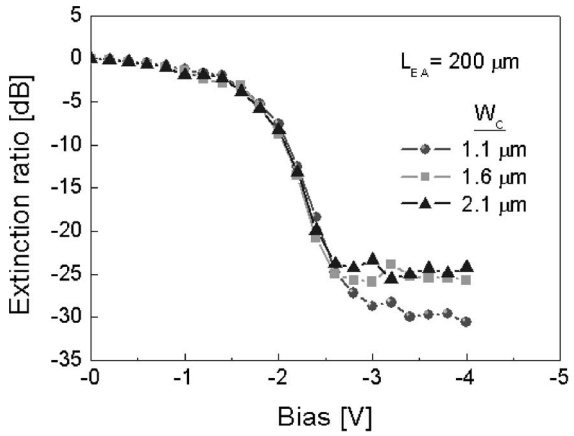

Fig. 8. Measured relative fiber-to-fiber ER characteristics for various MQW active-core widths.

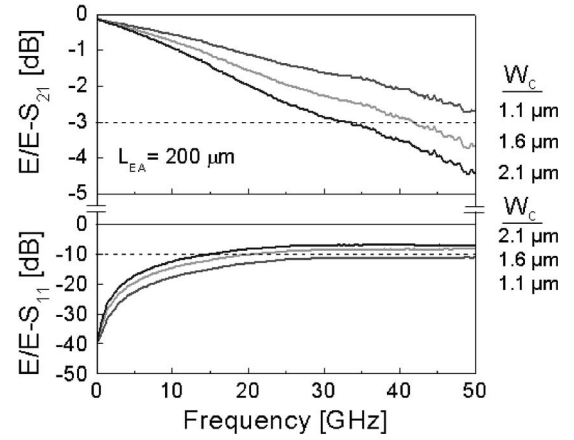

Fig. 9. Measured microwave transmission (S_{21}) and return loss (S_{11}) curves for 200-μm EAMs for various MQW active-core widths.

layer. Fig. 9 shows S_{21} and S_{11} curves for 200-μm EAMs with core width as a parameter. For the 2.1-μm-wide core, the E/E 3-dB-down bandwidth is as small as around 30 GHz, and the frequency at a return loss of -10 dB is about 15 GHz. However, as the core gets narrower, S_{21} and S_{11} improve dramatically.

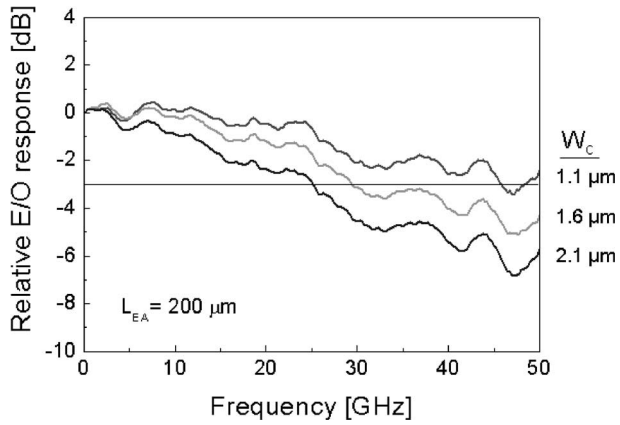

Fig. 10. Measured small-signal E/O frequency responses of the 200-μm EAMs for various MQW active-core widths.

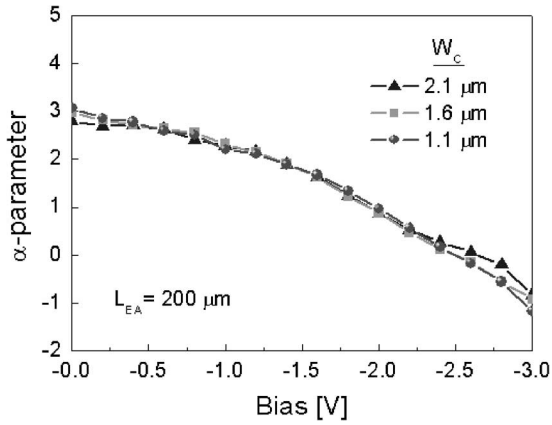

Fig. 11. Measured α parameters for various MQW active-core widths.

The E/E 3-dB-down bandwidth exceeds 50 GHz and the return loss is below -10 dB, even at that frequency. This clearly indicates that narrowing the core is a very effective way to improve the microwave-transmission characteristics.

Fig. 10 shows the measured small-signal E/O frequency responses of the 200-μm EAMs for various W_cs. For the 2.1-μm-wide core, the E/O 3-dB-down bandwidth is as small as about 25 GHz. However, as expected, the E/O 3-dB-down bandwidth increases with narrowing W_c, and it becomes as large as 46 GHz for W_c of 1.1 μm. Since Γ is almost constant until around W_c of 1 μm, the chirp parameter (α) given by $\Delta n/\Delta k$, where Δn and Δk are the increment of the real part and the imaginary part of the complex refractive index of the EAM, was expected to show no change with W_c. Fig. 11 shows α values for various MQW active-core widths measured by the fiber response method [17]. As expected, there is almost no change with decreasing W_c. This indicates that the narrowing W_c is very effective in increasing the E/O 3-dB-down bandwidth without sacrificing the important chirp parameter, which could be designed to have a negative value for long fiber transmission.

Fig. 12 shows the measured 40-Gb/s driver and optical eye diagram. Eye opening with an RF ER of 10.5 dB was successfully observed, even with a peak-to-peak voltage as low as

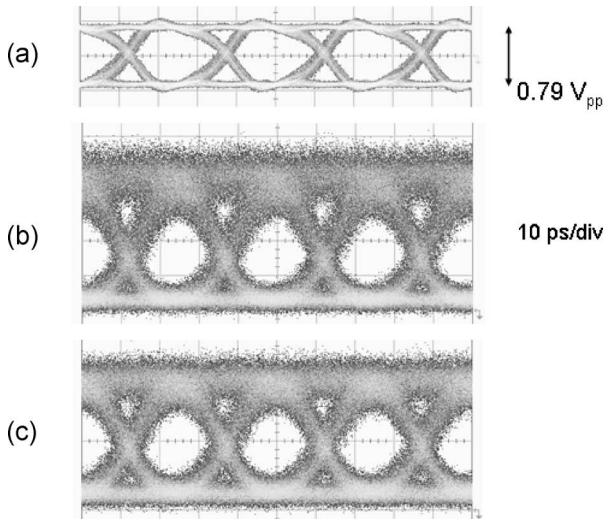

Fig. 12. Measured 40-Gb/s driver and optical eye diagrams. (a) Driver eye diagram. (b) Optical eye diagram at $V_{\rm bias}$ of -2.2 V. (c) Optical eye diagram at $V_{\rm bias}$ of -2.05 V.

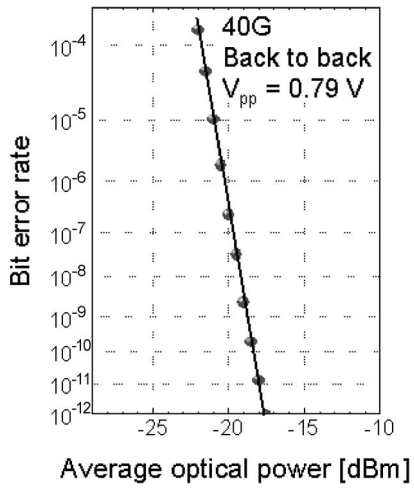

Fig. 13. Measured bit error rate for 40-Gb/s NRZ signal with 0.79-V driving voltage.

0.79 V with the device under -2.2-V bias and 50-Ω termination conditions [Fig. 12(b)]. Since the ON-state side has not sufficiently reached the saturation region of the extinction characteristics for the 0.79-V-swing amplitude of driver voltage, the upper band of the eye pattern signal is large. Somewhat enlarging the swing amplitude or moving a bias point to low voltage slightly makes the swing start from the saturation region and thereby improves the eye pattern. Fig. 12(c) shows the optical eye diagram of the device under -2.05-V bias condition as an example. The upper band is reduced, however, the ER becomes 8.3 dB. The dominant reason for the remaining excess jitter compared with that of the driver signal is thought to be the optical axis fluctuation arising from the on-chip measurement using lensed-fiber coupling with both input and output facets. The measured bit error rate for a 40-Gb/s nonreturn-to-zero (NRZ) pseudorandom-binary-sequence pulse pattern of 2^7-1 signal with 0.79-V driving voltage under -2.2-V bias is shown in Fig. 13. Error-free operation is confirmed.

V. Summary

We have successfully demonstrated a very-low-driving-voltage EAM operating at 40 Gb/s. A low-driving-voltage operation is led by employing tensile-strained InGaAlAs/InAlAs MQW layers having excellent extinction characteristics and by widening the 3-dB bandwidth. The wide $f_{3\,\rm dB}$ is achieved by reducing the MQW core width and using a polyimide-buried device structure with a low-loss microwave feed line. The successfully fabricated 40-Gb/s InGaAlAs/InAlAs EAM exhibits very good extinction characteristics. A narrow core buried with polyimide boosts the 3-dB bandwidth up to 46 GHz, even for a 200-μm EAM without degrading the ER. We performed 40-Gb/s NRZ transmission experiments. This EAM shows eye opening with an RF ER of 10.5 dB and error-free operation at a driving voltage as low as 0.79 V.

Acknowledgment

The authors thank Y. Noguchi for his technical support and T. Saito for his helpful discussions and support. They are also grateful to Y. Hasumi and H. Itoh for their encouragement throughout this paper.

References

[1] D. G. Moodie, A. D. Ellis, P. J. Cannard, C. W. Ford, A. H. Barrell, R. T. Moore, S. D. Perrin, R. I. McLaughlin, and F. Garcia, "40 Gb/s modulator with low drive voltage and high optical output power," in *Proc. 27th ECOC*, 2001, pp. 332–333.

[2] H. Feng, T. Makino, S. Ogita, H. Maruyama, and M. Kondo, "40 Gb/s electro-absorption-modulator-integrated DFB laser with optimized design," in *Proc. OFC*, 2002, pp. 340–341.

[3] Y. Miyazaki, H. Tada, S. Tokizaki, K. Takagi, Y. Hanamaki, T. Aoyagi, and Y. Mitsui, "Small-chirp 40 Gbps EA modulator with novel tensile-strained asymmetric quantum well absorption layer," presented at the Proc. 28th ECOC, 2002, Paper 10.5.6.

[4] W.-J. Choi, A. E. Bond, J. Kim, J. Zhang, R. Jambunathan, H. Foulk, S. O'Brien, J. V. Norman, D. Vandegrift, C. Wanamaker, J. Shakespeare, and H. Cao, "Low insertion loss and low dispersion penalty InGaAsP quantum-well high-speed electroabsorption modulator for 40-Gb/s very-short-reach, long-reach, and long-haul applications," *J. Lightw. Technol.*, vol. 20, no. 12, pp. 2052–2056, Dec. 2002.

[5] B. Mason, A. Ougazzaden, C. W. Lentz, K. G. Glogovsky, C. L. Reynolds, G. J. Przybylek, R. E. Leibenguth, T. L. Kercher, J. W. Boardman, M. T. Rader, J. M. Geary, F. S. Walters, L. J. Peticolas, J. M. Freund, S. N. G. Chu, A. Sirenko, R. J. Jurchenko, M. S. Hybertsen, L. J. P. Ketelsen, and G. Raybon, "40-Gb/s tandem electroabsorption modulator," *IEEE Photon. Technol. Lett.*, vol. 14, no. 1, pp. 27–29, Jan. 2002.

[6] M. Shirai, H. Arimoto, K. Watanabe, A. Taike, K. Shinoda, J. Shimizu, H. Sato, T. Ido, T. Tsuchiya, M. Aoki, S. Tsuji, N. Sasada, S. Tada, and M. Okayasu, "40 Gb/s electroabsorption modulators with impedance-controlled electrode," *Electron. Lett.*, vol. 39, no. 9, pp. 733–735, May 2003.

[7] K. Prosyk, R. Moore, I. Betty, R. Foster, J. Greenspan, P. Singh, S. O'Keefe, J. Ooosterom, and P. Langlois, "Low loss, low chirp, low voltage, polarization independent 40 Gb/s bulk electro-absorption modulator module," in *Proc. OFC*, 2003, vol. 1, pp. 269–270.

[8] H. Kawanishi, T. Suzuki, K. Nakamura, N. Mineo, Y. Shibuya, K. Sasaki, K. Yamada, and H. Wada, "1.3 μm EAM-integrated DFB lasers for 40 Gb/s very-short-reach application," in *Proc. OFC*, 2003, vol. 1, pp. 270–271.

[9] R. Lewen, S. Irmscher, U. Westergren, L. Thylen, and U. Eriksson, "Segmented transmission-line electroabsorption modulators," *J. Lightw. Technol.*, vol. 22, no. 1, pp. 172–179, Jan. 2004.

[10] G. Freeman, M. Meghelli, Y. Kwark, S. Zier, A. Rylyakov, M. A. Sorna, T. Tanji, O. M. Schreiber, K. Walter, J.-S. Rieh, B. Jagannathan, A. Joseph, and S. Subbanna, "40-Gb/s circuits built from a 120-GHz fT SiGe technology," *IEEE J. Solid-State Circuits*, vol. 37, no. 9, pp. 1106–1114, Sep. 2002.

[11] M. Tamura, T. Yamanaka, H. Fukano, Y. Akage, Y. Kondo, and T. Saitoh, "High-speed electroabsorption modulators buried with ruthenium-doped SI-InP," *IEEE Photon. Technol. Lett.*, vol. 16, no. 12, pp. 2613–2615, Dec. 2004.
[12] Y. Akage, H. Takeuchi, K. Tsuzuki, S. Kondo, Y. Noguchi, H. Okamoto, and T. Yamanaka, "Polarization-independent InGaAlAs/InAlAs electroabsorption modulators with an optimized strained-MQW," in *Proc. CLEO Pacific Rim*, 1999, pp. 191–192.
[13] H. Takeuchi, K. Tsuzuki, K. Sato, M. Yamamoto, Y. Itaya, A. Sano, M. Yoneyama, and T. Otsuji, "Very high-speed light-source module up to 40 Gb/s containing an MQW electroabsorption modulator integrated with a DFB laser," *IEEE J. Sel. Topics Quantum Electron.*, vol. 3, no. 2, pp. 336–343, Apr. 1997.
[14] T. Yamanaka, H. Fukano, and T. Saitoh, "Lightwave-microwave unified analysis of electroabsorption modulators integrated with RF coplanar waveguides," *IEEE Photon. Technol. Lett.*, vol. 17, no. 12, pp. 2562–2564, Dec. 2005.
[15] I.-H. Tan, C.-K. Sun, K. S. Giboney, J. E. Bowers, E. L. Hu, B. I. Miller, and R. J. Capik, "120-GHz long-wavelength low-capacitance photodetector with an air-bridged coplanar metal waveguide," *IEEE Photon. Technol. Lett.*, vol. 7, no. 12, pp. 1477–1479, Dec. 1995.
[16] K. Kato, A. Kozen, Y. Muramoto, Y. Itaya, T. Nagatsuma, and M. Yaita, "110-GHz, 50%-efficiency mushroom-mesa waveguide p-i-n photodiode for a 1.55-μm wavelength," *IEEE Photon. Technol. Lett.*, vol. 6, no. 6, pp. 719–721, Jun. 1994.
[17] F. Devaux, Y. Sorel, and J. F. Kerdiles, "Simple measurement of fiber dispersion and of chirp parameter of intensity modulated light emitter," *J. Lightw. Technol.*, vol. 11, no. 12, pp. 1937–1940, Dec. 1993.

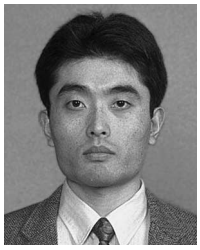

Hideki Fukano received the B.E. and M.E. degrees in electrical and electronic engineering from Toyohashi University of Technology, Toyohashi, Japan, in 1982 and 1984, respectively, and the Dr. Eng. degree from the Tokyo Institute of Technology, Tokyo, Japan, in 1994.

He joined the Nippon Telegraph and Telephone (NTT) Electrical Communications Laboratories, Kanagawa, Japan, in 1984. Since then, he has been engaged in research on heterojunction bipolar transistors (HBTs), heterojunction phototransistors (HPTs), laser diodes, photodiodes, and high-speed receiver optoelectronic integrated circuits (OEICs) composed of InP material systems. He is currently a Senior Research Engineer of the NTT Photonics Laboratories, where he is conducting research on high-speed electroabsorption modulators (EAMs) and EAM-integrated distributed-feedback lasers.

Dr. Fukano is a member of the Japan Society of Applied Physics and the Institute of Electronics, Information, and Communication Engineers (IEICE) of Japan.

Takayuki Yamanaka was born in Tochigi, Japan, in 1963. He received the B.S., M.S., and Ph.D. degrees from Hokkaido University, Sapporo, Japan, in 1986, 1988, and 1997, respectively, all in applied physics.

In 1988, he joined NTT Optoelectronics Laboratories, Kanagawa, Japan. He is now with NTT Photonics Laboratories and has been engaged in design and physics of semiconductor lasers and modulators. From 1998 to 1999, he stayed at the University of Waterloo, Waterloo, ON, Canada, and McMaster University, Hamilton, ON, as a Visiting Scholar.

Dr. Yamanaka is a member of the American Physical Society and the IEICE of Japan.

Munehisa Tamura was born in Chiba, Japan, on July 16, 1969. He received the B.E., M.E., and Ph.D. degrees from the Tokyo Institute of Technology, Tokyo, Japan, in 1993, 1995, and 1998, respectively, all in physical electronics.

He joined the Optoelectrics Laboratories of NTT Corporation, Kanagawa, Japan, in 1998. He has engaged in the research on integrated semiconductor optical devices and silica-based waveguide devices at the NTT Photonics Laboratories.

Dr. Tamura is a member of the Japan Society of Applied Physics and the IEICE of Japan.

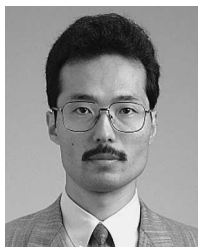

Yasuhiro Kondo was born in Nagasaki, Japan, in 1961. He received the B.S. degree from Kumamoto University, Kumamoto, Japan, in 1984 and the M.S. degree in physics and the Ph.D. degree in electronic device engineering from Kyushu University, Fukuoka, Japan, in 1986 and 1999, respectively.

In 1986, he joined NTT Optoelectronics Laboratories, Kanagawa, Japan, where he has been engaged in research on metal–organic vapor phase epitaxy (MOVPE) growth of III–V semiconductors and development of semiconductor lasers for transmission. He is now with NTT Photonics Laboratories.

Dr. Kondo is a member of the IEEE Lasers and Electrooptics Society (LEOS) and the Japan Society of Applied Physics.